Near-threshold vibrational excitation of acetylene by positron impact

Eliane M. de Oliveira and Marco A. P. Lima
Instituto de Física Gleb Wataghin, Universidade Estadual de Campinas, 13083-970 Campinas, São Paulo, Brazil

Sergio d'A. Sanchez* and Márcio T. do N. Varella†
Universidade Federal do ABC, Centro de Ciências Naturais e Humanas, Rua Santa Adélia 166, 09210-170 Santo André, Brazil

(Received 1 October 2009; published 29 January 2010)

We report vibrational excitation cross sections for C–C and C–H symmetric stretch modes of acetylene by positron impact. The contribution of these infrared inactive modes to the annihilation parameter is also addressed. The Feshbach projection operator approach was employed to vibrationally resolve e^+-acetylene scattering phase shifts obtained with the Schwinger multichannel method. The present results point out a virtual state pole at the equilibrium geometry of acetylene that becomes a bound state as either bond is stretched, in qualitative agreement with previous calculations for small hydrocarbons. The vibrational couplings are stronger for the C–C mode, giving rise to a bound state pole within the Franck-Condon region of the vibrational ground state. These bound and virtual states give rise to sharp threshold structures (vibrational resonances) in both the vibrational excitation cross sections and the annihilation parameter (Z_{eff}). We found fair agreement between the present calculations and previously reported e^+-acetylene vibrational excitation cross sections.

DOI: 10.1103/PhysRevA.81.012712 PACS number(s): 34.80.Uv, 34.80.Gs, 34.80.Lx, 34.50.Ez

I. INTRODUCTION

Recent years have witnessed an increasing interest on low-energy antimatter physics and chemistry [1]. It is now widely appreciated that positrons are not only useful for fundamental studies covering QED tests, gravity on antiatoms, Bose-condensed positronium (Ps) gases, and astrophysics but also for scientific and technological applications ranging from material science to the probing of metabolic processes with positron emission tomography (see Ref. [2] for a review). Such progress is to a large extent based on the improvement of accumulation and manipulation techniques that have allowed for bright low-energy antimatter beams [3].

A major advance in the field was the experimental evidence of vibrationally enhanced positron annihilation in molecular gases [4,5] that brought a lot of attention to positron-nucleus couplings in collision processes. Though considerable knowledge has been gained from annihilation theories and models [6–8], the *ab initio* description of positron interactions with large polyatomics is still challenging and details of the annihilation mechanism are yet to be unveiled. In this sense, computational studies of small hydrocarbons would be of key importance since they form low-energy metastable states with positrons [9,10] that can transfer energy into the nuclear degrees of freedom, thus enhancing the annihilation rates.

We recently implemented a computational method to vibrationally resolve positron-molecule collisions wherein bound and virtual states are found [11]. This approach is based on the Feshbach projection operator formalism [12], a well-known tool of electron-molecule scattering that has also proved useful for description of positron scattering and annihilation [8,11]. In this work, the method is applied to positron-impact vibrational excitation of symmetry-preserving modes of acetylene, namely C–C and C–H stretch. The well-known e^+-acetylene virtual state is significantly coupled to vibrations and becomes a bound state as the molecule is stretched, in agreement with independent calculations [10]. In addition to the inherent interest on vibrational excitation, state-to-state cross sections may help the development of annihilation theories. The connection between vibrational resonances in the annihilation parameter (Z_{eff}) and the total (vibrationally summed) cross section was recently pointed out [8], and state-to-state excitation cross sections might provide finer tests of theoretical approaches, since Z_{eff} is inherently vibrationally summed (i.e., it cannot be resolved in state-to-state transitions). Finally, though the infrared inactive modes addressed here do not have a clear signature in the experimental annihilation rate [5] we briefly discuss vibrationally resolved Z_{eff} estimates for these modes.

This paper is organized as follows. The theoretical and computational frameworks are outlined in Secs. II and III, respectively. The vibrational couplings and cross sections as well as model results for the annihilation parameter are discussed in Secs. IV and V. Our conclusions are summarized in Sec. VI.

II. THEORY

A. Feshbach projection operator approach

The application of the Feshbach projection operator (FPO) formalism [12] to vibrationally resolved collisions is discussed in detail elsewhere [13,14], so we only outline its main features. By decomposing the scattering wave function into discrete and continuum components, with the former embedded and coupled to the latter, the collision is described as the formation of a temporary positron-molecule compound: A positron in the continuum has a finite probability of capture in the discrete state, which eventually decays to the continuum by positron detachment. The nuclei, initially in the potential surface of the isolated target, are launched onto the potential surface of the transient, and long-lived compounds may allow

*Permanent address: Departamento de Física, UFPR, CP 19044, 81531-090 Curitiba, Paraná, Brazil.
†marcio.varella@ufabc.edu.br

for significant energy transfer into the vibrational degrees of freedom. The vibrational excitation integral cross section is given by

$$\sigma_{\nu_i\to\nu_f} = \frac{\pi}{k_i^2}\left| T^{\rm bg}_{\nu_i\nu_f} + \langle\eta_{\nu_f}|\Gamma^{1/2}(E_f) \times \frac{1}{E-K-V_{\rm opt}(E-H_N)}\Gamma^{1/2}(E)\,|\eta_{\nu_i}\rangle\right|^2, \quad (1)$$

where $E = k_i^2/2$ is the positron incident energy (with k_i the magnitude of the incident wave vector) and $T^{\rm bg}_{\nu_i\nu_f}$ is the background contribution to the $\eta_{\nu_i}\to\eta_{\nu_f}$ T-matrix element, where η_ν is a vibrational eigenstate of the target. K denotes the nuclear kinetic energy and $V_{\rm opt}$ is the complex and energy-dependent potential surface of the transient (the so-called optical potential [13]),

$$V_{\rm opt}(E-H_N) = V_0(q) + \epsilon_{\rm d}(q) + \Delta(E-H_N) - \frac{i}{2}\Gamma(E-H_N), \quad (2)$$

where a single vibrational coordinate (q) is assumed for simplicity. $H_N = K + V_0(q)$ is the vibrational Hamiltonian of the target (where V_0 is the potential energy surface of the electronic ground state) and $\epsilon_{\rm d}(q)$ is a potential energy shift related to positron capture (discrete state). The width Γ and the energy-dependent level shift Δ account for the discrete-continuum coupling,

$$\Gamma(E-H_N) = 2\pi\int kdk\int d\hat{\mathbf{k}}\,U_{\mathbf{k}}\,\delta\left(E-H_N-\frac{k^2}{2}\right)U^*_{\mathbf{k}}, \quad (3)$$

and

$$\Delta(E-H_N) = \frac{1}{2\pi}{\rm P}\int dE'\frac{\Gamma(E-H_N)}{E-E'}, \quad (4)$$

where the Cauchy principal value is indicated in Eq. (4). The FPO approach to positron annihilation is described elsewhere [8], and the angle-averaged annihilation parameter $Z_{\rm eff}$ is given by

$$Z_{\rm eff} = \frac{\pi}{k_i}\langle\eta_i|\frac{\Gamma^{1/2}(E)}{[E-K-V_{\rm opt}(E-H_N)]^\dagger} \times \rho_{\rm d}\,\frac{\Gamma^{1/2}(E)}{[E-K-V_{\rm opt}(E-H_N)]}|\eta_i\rangle, \quad (5)$$

where $\rho_{\rm d}(q)$ is the electron density at the positron. In obtaining Eq. (5), it was assumed that only the discrete component (trapped positron) contributes to the annihilation process, since a positron in the continuum would be weakly coupled to molecular vibrations and would have a low density at the target electrons.

B. Schwinger multichannel method

The complex potential of the positron-molecule transient can be obtained from fixed-nuclei scattering calculations performed for a number of target geometries. The Schwinger multichannel method (SMC), described in detail elsewhere [15], was employed in these calculations. The variational expression for the fixed-nuclei transition matrix is given by

$$t_{\mathbf{k}_i,\mathbf{k}_f}(E) = \sum_{m,n}\langle S_{\mathbf{k}_f}|V|\chi_m\rangle(d^{-1})_{mn}\langle\chi_n|V|S_{\mathbf{k}_i}\rangle, \quad (6)$$

where

$$d_{mn} = \langle\chi_m|(PVP + Q\hat{H}_{\rm ele}Q - VG_P^{(+)}V)|\chi_n\rangle. \quad (7)$$

In these expressions, $H_{\rm ele} = H_0 + V$ is the fixed-nuclei scattering Hamiltonian, where H_0 describes the noninteracting positron-molecule system, and V is the scattering potential. P is a projector onto the energy-allowed target electronic channels (comprising only the ground state in the present application), $Q = (1-P)$ is the closed-space projector, $G_P^{(+)}$ is the free-particle Green's function projected onto P space, and $\hat{H}_{\rm ele} = E - H_{\rm ele}$. $S_{\mathbf{k}}$ is an eigenstate of H_0, and the $(N+1)$-particle configuration state functions χ_m (which are products of target electronic states and projectile scattering orbitals) provide the basis for expansion of the trial scattering wave function. The dynamical response of the target electrons to the projectile field (correlation-polarization effects) is accounted for through the Q space (virtual excitations of the target).

C. Complex potential parametrization

The optical potential in Eqs. (1) and (5) depends on the collision energy and vibrational coordinates. Since the energy dependence would be important in near-threshold scattering [13], we account for the position dependence numerically and employ a model parametrization similar to those proposed in Refs. [16,17] to analytically describe the energy dependence of the complex potential. The decomposition of the fixed-nuclei T matrix is equivalent to the decomposition of the fixed-nuclei eigenphase sum [18],

$$\delta(E) = \delta_{\rm bg}(E) + \delta_{\rm d}(E), \quad (8)$$

with

$$\delta_{\rm d}(E) = \tan^{-1}\left(\frac{\frac{1}{2}\Gamma(E)}{E-\epsilon_{\rm d}-\Delta(E)}\right), \quad (9)$$

and the following model form is assumed for the width:

$$\Gamma(E) = \sum_{\alpha=1}^{n} A_\alpha E^{1/2}\exp(-b_\alpha E) \equiv \sum_{\alpha=1}^{n}\Gamma_\alpha. \quad (10)$$

A_α and b_α are model parameters and the Wigner threshold law [19] has been imposed on the assumption that near-threshold scattering is dominated by the s wave ($l=0$). The level shift may be readily obtained in closed form from Eqs. (4) and (10),

$$\Delta(E) = \Delta_0 + \frac{1}{2}\sum_{\alpha=1}^{n}\Gamma_\alpha\,|{\rm erf}(i\sqrt{b_\alpha E})|, \quad (11)$$

where erf denotes the error function and

$$\Delta_0 = -\frac{1}{2}\sum_{\alpha=1}^{n}\frac{A_\alpha}{\sqrt{\pi b_\alpha}}. \quad (12)$$

The background eigenphase is described with the leading term of the threshold expansion,

$$\delta_{\rm bg}(E) = aE^{1/2}, \quad (13)$$

where a is a model parameter. The discrete-state potential energy shift (ϵ_d) is also viewed as a model parameter, so the eigenphase sum at any given geometry is expressed in terms of $(2n+2)$ parameters, namely a, $\{A_\alpha\}$, $\{b_\alpha\}$, and ϵ_d. These are obtained from least-squares fits of Eq. (8) to SMC eigenphases, and the dependence of the optical potential on the nuclear coordinates is numerically described by interpolating the model parameters over the range of molecular geometries of interest. The operators in Eqs. (1) and (5) may therefore be represented in the basis of the vibrational eigenstates of the target $\{\eta_\nu\}$ (see Ref. [11] for details), such that

$$\sigma_{\nu_i\to\nu_f} = \frac{\pi}{k_i^2}\left| T^{\rm bg}_{\nu_i\nu_f} + \sum_{\nu\mu}\Gamma^{1/2}_{f\mu}(E_f)[\mathcal{D}^{-1}]_{\mu\nu}\Gamma^{1/2}_{\nu i}(E)\right|^2, \quad (14)$$

with

$$\mathcal{D}_{\mu\nu} = \langle\eta_\mu|[E-K-V_{\rm opt}(E-H_N)]|\eta_\nu\rangle, \quad (15)$$

$$\Gamma_{\mu\nu}(E-H_N) = \sum_j \langle\eta_\mu|\Gamma^{1/2}(E-\varepsilon_j)|\eta_j\rangle \times \langle\eta_j|\Gamma^{1/2}(E-\varepsilon_j)|\eta_\nu\rangle \quad (16)$$

and

$$\Delta_{\mu\nu}(E-H_N) = \frac{1}{2\pi}\sum_j {\rm P}\int dE' \times \frac{\langle\eta_\mu|\Gamma^{1/2}(E'-\varepsilon_j)|\eta_j\rangle\langle\eta_j|\Gamma^{1/2}(E'-\varepsilon_j)|\eta_\nu\rangle}{E-E'}. \quad (17)$$

In these expressions, ε_j is a vibrational eigenvalue of the target, and the annihilation parameter can be expressed in a similar fashion,

$$Z_{\rm eff} = \frac{\pi}{k_i}\rho_d \sum_{\nu\mu}\Gamma^{1/2}_{i\mu}[\mathcal{D}^{\dagger-1}]_{\mu\nu}[\mathcal{D}^{-1}]_{\nu\mu}\Gamma^{1/2}_{\mu i}, \quad (18)$$

where the density ρ_d is calculated at the equilibrium geometry of the target; that is, its dependence on the vibrational coordinate is neglected, $\langle\eta_\mu|\rho_d|\eta_\nu\rangle \simeq \delta_{\mu\nu}\,\rho_d(q_{\rm eq})$.

III. COMPUTATIONAL PROCEDURES

A. Fixed-nuclei calculations

The target electronic ground state was described at the restricted Hartree-Fock (HF) level with a $5s3p1d$ basis set on carbon atoms, $3s1p$ on hydrogen atoms, and $1s1p1d$ on the center of mass (the details of which are given elsewhere [20]). The scattering basis set was augmented with s-, p-, and d-type functions on dummy centers located at the corner of a cube. The equilibrium bond lengths $r_{\rm CC} = 2.233a_0$ and $r_{\rm CH} = 1.998a_0$ were obtained with the HF potential, and the target was treated as a D_{2h} molecule due to limitations of our computer codes. Correlation-polarization effects were accounted for by including all singly excited target states (from valence hole orbitals) in the closed space, giving rise to 6053 configurations to expand the scattering wave function.

The frequencies and reduced masses of the normal modes were also obtained from the HF potential [21]. The calculated values were 2216 $\rm cm^{-1}$ and 3.630 g/mol for C–C stretch, and 3660 $\rm cm^{-1}$ and 1.250 g/mol for C–H stretch. For the C–C mode, scattering calculations were performed for $q_{\rm CC} = -0.500a_0, -0.350a_0, -0.200a_0, -0.100a_0, -0.050a_0, -0.025a_0, 0.000a_0, 0.025a_0, 0.050a_0, 0.075a_0, 0.100a_0, 0.125a_0, 0.150a_0, 0.200a_0, 0.275a_0, 0.350a_0, 0.500a_0$, and $0.650a_0$, where $q_{\rm CC} = 0.000$ is the equilibrium geometry. For C–H stretch, fixed-nuclei calculations were performed at $q_{\rm CH} = -0.500a_0, -0.350a_0, -0.200a_0, -0.100a_0, -0.050a_0, 0.000a_0, 0.050a_0, 0.100a_0, 0.150a_0, 0.175a_0, 0.200a_0, 0.225a_0, 0.250a_0, 0.275a_0, 0.300a_0, 0.325a_0, 0.350a_0, 0.375a_0, 0.400a_0, 0.500a_0$, and $0.650a_0$. For all geometries, the projectile energies were taken from 10^{-4} to 3.0 eV.

B. Vibrational excitation cross sections

The operators and wave functions were represented on evenly spaced 256-point grids for both modes. A six-parameter model, corresponding to $n = 2$ in Eq. (10), was employed to represent the $l = 0$ eigenphase, and the deviations between least-squares fits and SMC eigenphases were typically 2%–3% (with the maximum deviation not exceeding 5%). The target vibrational eigenstates were obtained from the HF potentials by employing the energy screening technique [22], and the $0\to 0, 1, 2$ cross sections were well converged with the representation of the nonlocal operator truncated at $\nu = 9$. The energy integration in Eq. (17) was performed with Gauss-Legendre quadratures for three intervals defined from the position of the pole ($E_{\rm pole} = E$) as follows: $0 \leqslant E' < E$, $E < E' < 2E$, and $E' > 2E$. This procedure ensured that the quadrature points were evenly distributed below and above the poles, thus avoiding significant errors. The convergence of this numerical integration was crucial to obtain accurate vibrational cross sections near the thresholds (see the following).

IV. RESULTS

The s-wave phase shifts obtained from fixed-nuclei SMC calculations and the corresponding least-squares fits are shown in Fig. 1 for geometries given in Sec. III A, where results for the C–C and C–H stretch modes are shown in the upper and lower panels, respectively. For both modes, the threshold behavior indicates the formation of bound states as the bonds are stretched, since $\delta(E\to 0)\to\pi$ would be expected for such states [23]. In view of the large scattering lengths, the behavior of the phase shifts can be understood on the basis of effective range theory, such that negative slopes at very low energies indicate bound states,

$$\delta_0(k) \simeq \pi - k\alpha, \quad (19)$$

where $\alpha > 0$ is the scattering length and k is the positron momentum. Positive slopes point out virtual states ($\alpha < 0$),

$$\delta_0(k) \simeq -k\alpha = k|\alpha|, \quad (20)$$

where the relation between the scattering lengths and the poles on the imaginary axis of the complex k plane ($\pm i\kappa_0$),

$$\alpha = \pm\frac{1}{\kappa_0}, \quad (21)$$

make clear that the slopes should be larger for shallower poles (i.e., smaller κ_0). The SMC phase shifts shown in Fig. 1 show

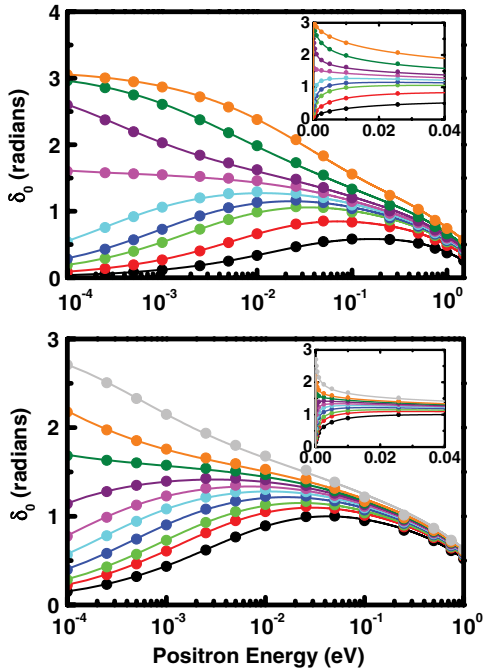

FIG. 1. (Color online) Fixed-nuclei s-wave scattering phase shifts (δ_0). The lines are least-squares fits of Eq. (8) to SMC calculations (circles). Results for the C–C and C–H symmetric stretch modes are shown in the upper and lower panels, respectively, and the different curves correspond to selected geometries. For both modes, the low-energy eigenphases (also shown in the insets) monotonically increase as the bonds are stretched.

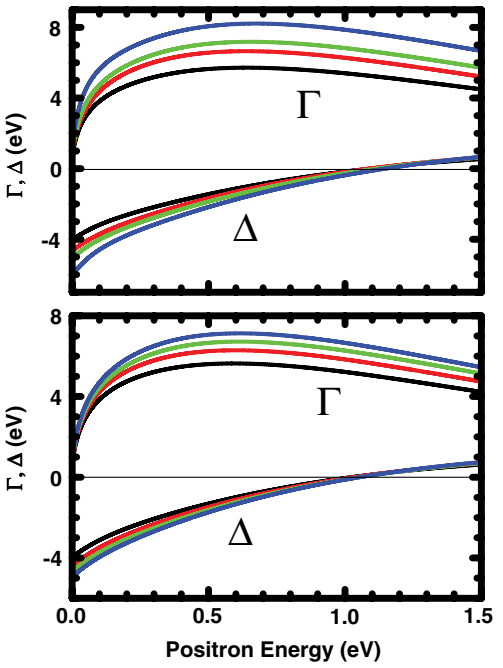

FIG. 2. (Color online) Fixed-nuclei level shifts (Δ) and widths (Γ) for selected geometries. Results for the C–C and C–H symmetric stretch modes are shown in the upper and lower panels, respectively. For both modes, the width peak heights around 0.6 eV monotonically increase with the bond lengths, while the level shift at zero energy is monotonically decreasing.

clear signatures of virtual states becoming bound states as the molecular bonds are stretched (i.e., the potential becomes more attractive the more stretched the molecule is).

The corresponding level shifts (Δ) and widths (Γ) are shown in Fig. 2 for the C–C (upper panel) and C–H (lower panel) modes. The parametric dependence on the vibrational coordinates may be easily followed since the width peak heights monotonically increase with the bond lengths, while the level shift at zero energy is monotonically decreasing (a tendency that is inverted at higher energies due to the crossings around 1.1 eV).

The phase shifts in Fig. 1 suggest that the threshold behavior of elastic and vibrationally inelastic cross sections would result from low-lying virtual and bound states. To survey the trajectory of these poles in the complex momentum plane, an advantage may be taken from the analytical model employed for the energy dependence of the complex potential. Virtual and bound states show up as singularities on the negative and positive imaginary axis of the complex k plane, respectively [23]. These can be obtained from the analytic continuation of the complex potential [16,17] and correspond to the zeros of

$$E - \epsilon_{\rm d} - \Delta(E) - \frac{i}{2}\Gamma(E) = 0. \qquad (22)$$

On the imaginary axis, one finds $\Gamma = 0$ and

$$\Delta(-|E|) = \Delta_0 \pm \sum_{\alpha=1}^{n} |E|^{1/2} \exp(b_\alpha |E|)\, \mathrm{erfc}(\sqrt{b_\alpha |E|}), \qquad (23)$$

where the $\pm$ sign on the right-hand side of Eq. (23) correspond to the $\pm ik$ branches. As a result, the intersections of the straight line $(E - \epsilon_{\rm d})$ with the plus (minus) branch indicates the bound (virtual) states, as shown in Fig. 3. The pole trajectories as functions of the vibrational coordinates are shown in Fig. 4, along with the probabilities of the vibrational ground states of both modes. Though the virtual state at the equilibrium geometry becomes a bound state for longer bond lengths in both cases, the slope of the C–C mode trajectory is considerably larger, giving rise to a bound state within the Franck-Condon region of the vibrational ground state. The C–H mode pole, on the other hand, has a virtual state character

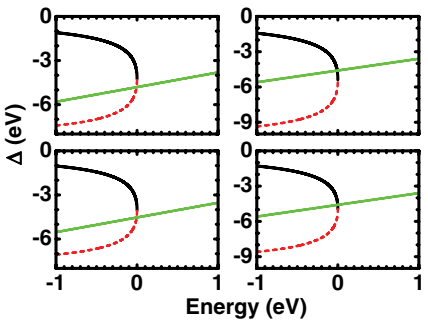

FIG. 3. (Color online) Bound-state (solid black lines) and virtual-state (dashed red lines) branches of the the level shift (Δ). Selected results are shown for the C–C (upper panels) and C–H (lower panels) stretch modes. Pole energies are obtained from the crossings of the branches with the $E - \epsilon_{\rm d}$ straight lines (with virtual and bound states in the left and right panels, respectively).

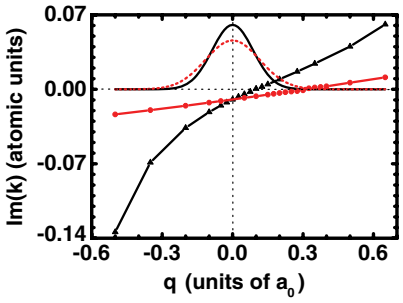

FIG. 4. (Color online) Pole trajectories in the complex momentum plane for the C–C (black triangles) and C–H (red circles) symmetric stretch modes. Bound and virtual states are found in the positive ($+ik$) and negative ($-ik$) half-planes, respectively. The probability densities of the vibrational ground states are also indicated in the upper plane for the C–C (black solid line) and C–H (red dashed line) modes.

over a broad range of geometries. The $0 \rightarrow 1$ vibrational excitation cross sections are shown in the left panel (C–C mode) and right panel (C–H mode) of Fig. 5. Though both modes show threshold structures arising from the low-energy poles, the vibrational resonance of the C–C mode has a much greater strength.

V. DISCUSSION

Previous studies of positron scattering by small hydrocarbons [9,10], with the target molecules frozen in the equilibrium geometries, brought out the existence of virtual state poles. The calculations of Nishimura and Gianturco [10] also indicated that these poles become bound states as the C–H bond is stretched. These results, obtained with an independent computational framework, point out the same behavior reported here for the C–C and C–H stretch modes of acetylene (see Fig. 4). This is a relevant fact not only because this general trend is confirmed by the present results but also because the couplings of virtual state poles to molecular vibrations, though widely acknowledged in electron scattering [13,17,24], are often disregarded in positron-molecule collision models [6,7]. The present results also suggest that these couplings

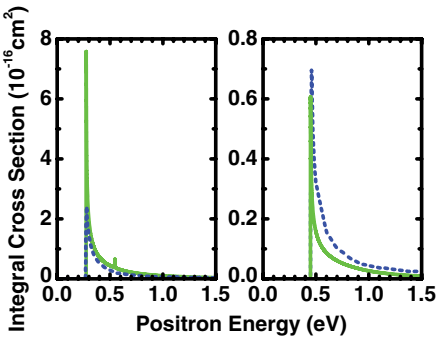

FIG. 5. (Color online) Integral cross section for the $0 \rightarrow 1$ vibrational excitation of the C–C (left panel) and C–H (right panel) symmetric stretch modes of acetylene by positron impact. Solid green lines: present results; dashed blue lines: calculation of Franz and Gianturco [27]. For the C–C mode, the small peak around 0.53 eV is a signature of the $0 \rightarrow 2$ channel threshold.

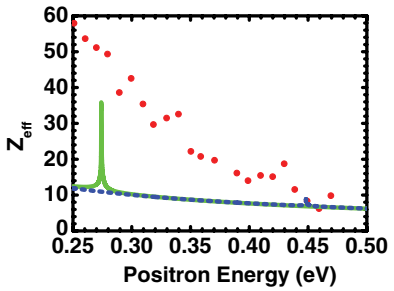

FIG. 6. (Color online) Model single-mode calculations for the annihilation parameter (Z_{eff}). Solid green line: C–C symmetric stretch mode; dashed blue line: C–H symmetric stretch mode; bullets: experimental data of Gilbert *et al.* [4] (rescaled by a factor of 0.1).

are stronger for the C–C mode, as indicated by the slope of the pole trajectory at the equilibrium geometry. Since longer bond lengths seem to better accommodate the positron, stretching the C–C triple bond should give rise to a more attractive e^+-acetylene potential due to its high electron density.

Model single-mode calculations for the annihilation parameter (Z_{eff}) are shown in Fig. 6, where the experimental data of Ref. [4] were rescaled by a factor of 0.1 for comparison purposes. The one-to-one correspondence between resonances in the vibrationally summed cross section and in the annihilation parameter was recently pointed out [8] and the present results illustrate that virtual state poles give rise to resonantly enhanced annihilation rates. It is well known that low-lying singularities in the fixed-nuclei scattering matrix give rise to vibrational resonances in the vicinity of elastic and inelastic thresholds when vibrations are included in the model [24] and these should also be present in the annihilation parameter. Though experimental results indicate that infrared active modes give rise to much stronger Z_{eff} resonances, the present results indicate that vibrationally enhanced annihilation should also arise from infrared inactive modes. Our results are not directly comparable to the experimental data [4] for a number of reasons, namely the complete neglect of infrared active modes and many-mode effects; the threshold shifts due to the HF description of the target potential energy surface; and the fact that partial waves other than $l = 0$ were not accounted for (since the experimental energy resolution, ~25 meV, is also much larger than the resonance widths and of the order of the vibrational energy spacings, the signature of symmetric stretch modes becomes blurred). Nevertheless, the existence of vibrational resonances is a relevant fact from a conceptual standpoint.

Finally, we would like to comment on the numerical convergence of the present results. As described in Sec. III B, the numerical energy integration of the level-shift operator in Eq. (17) was carried out with distinct Gauss-Legendre quadratures for three intervals, namely $0 \leqslant E' < E$, $E < E' < 2E$, and $E' > 2E$, where E is the pole energy. This procedure ensures that quadrature points are evenly distributed below and above the pole and was essential to attain numerically converged cross sections [25]. Though small quadratures were adequate at higher energies, a proper description of the threshold peaks in the vibrational excitation

cross sections (Fig. 5) could only be obtained with a total of nearly 1000 quadrature points. In addition, the energy grid for cross-section plots must be very dense around the threshold peaks (10^{-6} eV step), because the resonances are very narrow [$\Gamma(E) \sim 10^{-5}$–10^{-4} eV]. For these reasons, the present threshold peak for the C–C mode is significantly higher than in previously reported calculations [26], obtained with a total of nearly 150 quadrature points and energy steps of around 10^{-2} eV. The present cross sections also compare favorably with the body-frame vibrational close coupling estimates of Franz and Gianturco [27]. The major discrepancy is the peak height of the C–C mode excitation cross section, which should be very sensitive to small differences in the description of the e^+-acetylene interaction potential as well as to numerical aspects. Though we are not in position to criticize their model, the figures of Ref. [27] (in particular, the insets) suggest that energy grids with 10^{-2} eV steps were employed. It is possible that denser grids could favor the comparison with the present results.

VI. CONCLUSIONS

The Feshbach projection operator approach was employed to vibrationally resolve e^+-acetylene scattering phase shifts obtained with the SMC method. Vibrational excitation cross sections were calculated for the $0 \rightarrow 1$ transitions of the C–C and C–H symmetric stretch modes, and the contribution of these infrared inactive modes to the annihilation parameter was also discussed. In agreement with previous calculations for small hydrocarbons [10], the present results point out a virtual state pole at the equilibrium geometry of acetylene that becomes a bound state as either bond is stretched. Though this pole keeps its virtual state character over a fairly broad range of C–H bond lengths, stretching the C–C bond gives rise to a bound state in the vicinity of the equilibrium geometry, within the Franck-Condon region of the vibrational ground state. These poles give rise to sharp threshold structures (vibrational resonances) in both the vibrational excitation cross sections and the annihilations parameter Z_{eff}, as expected. The present vibrational excitation cross sections are in fair agreement with the calculations of Franz and Gianturco [27], the major discrepancy being the C–C mode threshold peak height.

ACKNOWLEDGMENTS

The calculations were partly performed at Centro Nacional de Processamento de Alto Desempenho (CENAPAD-SP). The authors acknowledge support from the Brazilian agencies Coordenação de Aperfeiçoamento de Pessoal de Nível Superior (CAPES), Conselho Nacional de Desenvolvimento Científico e Tecnológico (CNPq), and Fundação de Amparo à Pesquisa do Estado de São Paulo (FAPESP).

[1] C. M. Surko, Nature (London) **449**, 153 (2007).
[2] C. M. Surko, G. F. Gribakin, and S. J. Buckman, J. Phys. B **38**, R57 (2005).
[3] J. R. Danielson, T. R. Weber, and C. M. Surko, AIP Conf. Proc. **1037**, 84 (2008).
[4] S. J. Gilbert, L. D. Barnes, J. P. Sullivan, and C. M. Surko, Phys. Rev. Lett. **88**, 043201 (2002).
[5] L. D. Barnes, S. J. Gilbert, and C. M. Surko, Phys. Rev. A **67**, 032706 (2003); L. D. Barnes, J. A. Young, and C. M. Surko, *ibid.* **74**, 012706 (2006).
[6] G. F. Gribakin, Phys. Rev. A **61**, 022720 (2000); K. Iwata, G. F. Gribakin, R. G. Greaves, C. Kurz, and C. M. Surko, *ibid.* **61**, 022719 (2000).
[7] G. F. Gribakin and C. M. R. Lee, Phys. Rev. Lett. **97**, 193201 (2006).
[8] S. d'A. Sanchez, M. A. P. Lima, and M. T. do N. Varella, Phys. Rev. A **80**, 052710 (2009).
[9] C. R. C. de Carvalho, M. T. do N. Varella, M. A. P. Lima, and E. P. da Silva, Phys. Rev. A **68**, 062706 (2003).
[10] T. Nishimura and F. A. Gianturco, Phys. Rev. A **72**, 022706 (2005).
[11] M. T. do N. Varella and M. A. P. Lima, Phys. Rev. A **76**, 052701 (2007).
[12] H. Feshbach, Ann. Phys. (NY) **5**, 357 (1958); **19**, 287 (1962).
[13] W. Domcke, J. Phys. B **14**, 4889 (1981); Phys. Rep. **208**, 97 (1991).
[14] A. U. Hazi, T. N. Rescigno, and M. Kurilla, Phys. Rev. A **23**, 1089 (1981).
[15] J. S. E. Germano and M. A. P. Lima, Phys. Rev. A **47**, 3976 (1993).
[16] M. Berman, H. Estrada, L. S. Cederbaum, and W. Domcke, Phys. Rev. A **28**, 1363 (1983).
[17] H. Estrada and W. Domcke, J. Phys. B **18**, 4469 (1985).
[18] A. U. Hazi, Phys. Rev. A **19**, 920 (1979); M. Berman and W. Domcke, *ibid.* **29**, 2485 (1984).
[19] E. P. Wigner, Phys. Rev. **73**, 1002 (1948).
[20] C. R. C. de Carvalho, M. T. do N. Varella, E. P. da Silva, J. S. E. Germano, and M. A. P. Lima, Nucl. Instrum. Methods Phys. Res. B **171**, 33 (2000).
[21] M. J. Frisch *et al.*, GAUSSIAN 98, Revision A.7 (Gaussian, Inc., Pittsburgh, 1998).
[22] K. Takatsuka and N. Hashimoto, J. Chem. Phys. **103**, 6057 (1995).
[23] C. J. Joachain, *Quantum Collisions Theory* (North-Holland, Amsterdam, 1975).
[24] R. K. Nesbet, Phys. Rev. A **19**, 551 (1979); J. P. Gauyacq and A. Herzenberg, *ibid.* **25**, 2959 (1982).
[25] The convergence of the numerical energy integration can be easily checked by arbitrarily switching off the position dependence of the width operator in Eq. (17), since in this case the integration can be performed analytically.
[26] M. T. do N. Varella, E. M. de Oliveira, and M. A. P. Lima, Nucl. Instrum. Methods B **266**, 435 (2008).
[27] J. Franz and F. A. Gianturco, Eur. Phys. J. D **39**, 407 (2006).